Hundreds of antimicrobial peptides create a selective barrier for insect gut symbionts

Joy Lachat[1]†, Gaëlle Lextrait[1]†, Romain Jouan[1]†, Amira Boukherissa[1], Aya Yokota[1], Seonghan Jang[2]‡, Kota Ishigami[2], Ryo Futahashi[3], Raynald Cossard[1], Delphine Naquin[1], Vlad Costache[4], Luis Augusto[1], Pierre Tissière[1], Emanuele G. Biondi[1], Benoît Alunni[1]§, Tatiana Timchenko[1], Tsubasa Ohbayashi[1,5], Yoshitomo Kikuchi[2]*, Peter Mergaert[1]*

[1]Université Paris-Saclay, CEA, CNRS, Institute for Integrative Biology of the Cell (I2BC); Gif-sur-Yvette, 91198, France.

[2]Bioproduction Research Institute, National Institute of Advanced Industrial Science and Technology (AIST), Hokkaido Center; Sapporo, 062-8517, Japan.

[3]National Institute of Advanced Industrial Science and Technology (AIST); Tsukuba, 305-8566, Japan.

[4]MIMA2 Imaging Core Facility, Microscopie et Imagerie des Microorganismes, Animaux et Aliments, INRAE; Jouy-en-Josas, 78352, France.

[5]Institute for Agro-Environmental Sciences, National Agriculture and Food Research Organization (NARO); Tsukuba, 305-8604, Japan.

†Equal contribution

‡ Present address: Infectious Disease Research Center, Korea Research Institute of Bioscience and Biotechnology, Daejeon 34141, South Korea.

§Present address: Institut Jean-Pierre Bourgin, INRAE, AgroParisTech, Université Paris-Saclay; 78000 Versailles, France.

*To whom correspondence should be addressed: peter.mergaert@i2bc.paris-saclay.fr; y-kikuchi@aist.go.jp

Abstract

Members of gut microbiota are confronted by the epithelial immune system suggesting that resistance is crucial for chronical gut colonization. We show that the insect *Riptortus pedestris* produces massively hundreds of specific antimicrobial peptides (AMPs), the Crypt-specific Cysteine-Rich peptides (CCRs), in the posterior midgut that houses a mono-specific bacterial community. CCRs have membrane-damaging antimicrobial activity against diverse bacteria but gut symbionts have elevated resistance. Tn-seq determined the genetic repertoire in the gut symbiont *Caballeronia insecticola* to manage AMP stress, identifying novel pathways targeted by AMPs in addition to cell envelope functions. Mutants in the corresponding genes have reduced capacity to colonize the gut, demonstrating that CCRs create a selective barrier and resistance is a key attribute of gut symbionts.

Main text

The animal gut is colonized by large numbers of bacteria, which provide essential functions to the host (*1,2*). Their presence constitutes an immunological challenge and the intestinal epithelium responds to them with the activation of a diversified repertoire of immune effectors (*3,4*). The members of the microbiota have a coevolved relationship with this active immune system, enabling them to colonize the gut stably (*5,6*). Among the prominent immune mechanisms is the production of AMPs, which are secreted in the gut lumen and come in contact with the microbiota (*7-10*). Thus, gut commensals are expected to be resilient to AMPs (*11*) but how they adapt and how important this is for gut colonization remains largely unexplored.

The bean bug *Riptortus pedestris* has a particular gut organization, associated with a (nearly) mono-specific microbiota present in the specialized posterior midgut region M4 composed of two rows of crypts branched on a central tract (*12*). This microbiota is acquired from the environment through feeding. The M4 bacteria are very specific, belonging to the *Caballeronia* genus and are mostly present as a single colonizer, established through a multifaceted selection process (*13-16*). Among the bean bug colonizers, *Caballeronia insecticola* has emerged as a model species (*17*). We took advantage of this simplified gut-microbe interaction model to explore how gut bacteria are adapted to resist intestinal AMP challenge.

The *Riptortus pedestris* midgut produces hundreds of AMPs

A preliminary transcriptome analysis of the M4 midgut region has identified a novel class of secretory peptides, which we call the CCRs (*18,19*). In order to define the expression pattern of *CCR* genes, the transcriptome was determined by RNA-seq in midgut regions of insects that were reared for different times in the presence or absence of the *C. insecticola* gut symbiont (**Fig. 1A**). Hidden Markov Models based on the previously identified CCR sequences were used to identify in the newly generated transcriptome the complete set of CCR sequences. This analysis revealed 310 *CCR* transcripts (**data S1**). The encoded CCR peptides do not show high similarity apart from a pattern of conserved cysteine residues (**Fig. 1B**). Despite their sequence divergence, AlphaFold2 predicted similar folds for tested CCR peptides, consisting of three pairs of β-sheets that are probably connected by cystine bridges (**Fig. 1C**). Differential expression analysis revealed that the majority of the *CCR* genes are most strongly expressed in the midguts of symbiotic insects (**Fig. 1D**, **data S1**). Subsets of genes were specific for the M3, M4B and the majority for the M4 region carrying the *C. insecticola* bacteria, suggesting that the encoded peptides target the symbionts. Moreover, the *CCRs* are among the most strongly expressed transcripts in the overall transcriptome (**fig. S1**), suggesting a primordial role of the

peptides in the midgut. The *CCR* genes did not exhibit similarity to known sequences of other organisms. However the taxonomically restricted nature of the genes as well as the structure of the CCRs, being small, secreted and characterized by conserved cysteine residues, remind strongly to AMP gene families (*10*) and AMP prediction tools confirmed this presumption (**Fig. 1C**, **data S1**). Whole mount *in situ* hybridization with the infected-M4-specific gene *CCR0043* showed that the gene is expressed uniformly by the epithelial cells in all M4 crypts (**Fig. 1E**, **fig. S2**). This pattern contrasts with the mammalian small intestine where specialized cell types at the base of crypts express AMP genes (*20*).

Based on the expression pattern and the predicted AMP activity, we selected CCRs for chemical synthesis (**Fig. 1C**, **table S1**). These seven CCRs, together with thanatin and riptocin, two known innate immunity-related AMPs of *R. pedestris* (*21*), LL37 and NCR335, from mammal and plant origin respectively (*22*,*23*) and bacterial polymyxin B (PMB), were tested for growth inhibiting activity against a panel of taxonomically diverse bacterial species *Bacillus subtillis*, *Sinorhizobium meliloti*, *Paraburkholderia fungorum* and *C. insecticola*. The first two species are unable to colonize the *R. pedestris* midgut while the latter two can efficiently proliferate in the crypts (*13*). In agreement with the bioinformatics predictions, the CCRs had growth inhibiting activity against *B. subtilis* and *S. meliloti* although with variable strengths (**Fig. 2A,B**). On the other hand, the two species, *P. fungorum* and *C. insecticola*, that are able to colonize the gut crypts, are not or only weakly affected by the tested CCRs (**Fig. 2A,B**). This pattern of sensitivity/resistance to CCRs matches with the response of these species to PMB and in part to the other tested peptides. CFU counting showed the bacterial reduction from 10^7 CFU to no colonies after treatment of sensitive *S. meliloti* with the CCR1659 peptide for a few hours, indicating that the growth inhibition results from a bactericidal activity, similarly as for PMB (**Fig. 2C**). The bactericidal activity of CCR1659 was abolished by prior Proteinase K treatment of the peptide and inhibited by the presence of the divalent cations Ca^{2+} and Mg^{2+}, which interfere with the electrostatic interaction of AMPs with negatively charged membrane lipids and diminish the activity of membrane-targeting AMPs (*24*) (**Fig. 2C; fig. S3**). To acquire insight in the killing mode of CCR1659, we tested the hypothesis that the peptide disrupt bacterial membranes, like PMB and the other tested AMPs do (*25*-*27*). Outer and inner membrane integrities in *S. meliloti* were consecutively damaged by both CCR1659 and PMB treatment, as measured respectively by 1-N-PhenylNaphthylamine (NPN) and Propidium Iodide (PI) uptake leading to enhanced fluorescence (**Fig. 2D**). In agreement with the membrane disruption, fluorescence microscopy showed that FITC-modified CCR1659 labelled the

envelope of *S. meliloti* cells in a similar way as polylysine-FITC, which is a polycation known to interact with negatively charged membranes of bacteria (**Fig. 2E**) (*28,29*). Binding of CCR1659 to the envelope suggests that its killing efficiency depends on the strength of envelope binding. To test this assumption, we measured with flow cytometry the binding level of CCR1659-FITC and polylysine-FITC to the above panel of species. Strikingly, CCR1659-sensitive *S. meliloti* and *B. subtilis* were strongly labeled with these two molecules while resistant *C. insecticola* and *P. fungorum* only weakly (**Fig. 2F**). Thus, the level of binding to cells is correlated with the susceptibility/resistance pattern. Scanning electron microscopy (SEM) of CCR1659-treated *S. meliloti* cells further confirmed the membrane-perturbing activity of the peptide that provoked the leakage of fibrous materials from damaged cells similarly as PMB (**Fig. 2G; fig. S4**). Together, this data reveal that the M4 symbiotic region of the gut produces a remarkably large arsenal of CCR peptides with membrane-damaging AMP activity.

The *Caballeronia insecticola* genetic repertoire determining AMP resistance

Species that colonize the midgut display a high level of resistance to CCRs and other AMPs suggesting that resistance is a prerequisite for efficient gut colonization. To test this hypothesis, we aimed to identify the resistance determinants in *C. insecticola* and assess if they control gut colonization. A transposon mutant library (*30*) was used to perform a Tn-seq screen with PMB, since PMB has a similar membrane action as CCR peptides and is commercially accessible in sufficient quantities for Tn-seq experiments. The screen, performed with three sub-lethal PMB concentrations, resulted in 54 genes whose mutation provoked a fitness defect with the highest concentration. With the lower PMB concentrations, subsets of these genes were identified suggesting a multifactorial resistance with some mechanisms contributing more strongly than others (**Fig. 3A,B**; **fig. S5, data S2**). In agreement with the membrane-targeting mode of action of PMB, the majority of fitness genes are involved in the generation of bacterial envelope components, including LPS, peptidoglycan, phospholipids, hopanoids and membrane protein machineries. In order to validate the Tn-seq results, we constructed insertion and deletion mutants in 11 genes selected among the 54 PMB fitness genes. These genes are predicted to be involved in the biosynthesis of the LPS core (*dedA*, *waaC* and *waaF*)(*31-33*), LPS O-antigen (*wbiF*, *wbiG*, *wbiI*, *wzm* and *rfbA*)(*34*), peptidoglycan (*dedA*), membrane protein machineries (*tolB* and *tolQ*) (*35,36*), in addition to a gene (*tpr*) encoding a tetratricopeptide repeat protein of unknown function. Complementing strains were constructed for some of the mutants. Sensitivity assays with PMB and colistin (COL), another polymyxin-family AMP, confirmed

that each mutant had an 8- to 32-fold increased sensitivity compared to the WT (**Fig. 3C**) while the complemented mutants were restored to WT-levels (**fig. S6**). Thus, the Tn-seq analysis correctly identified genetic determinants for PMB resistance in *C. insecticola*.

In line with the sensitivity of the mutants to PMB and the membrane-attacking properties of CCRs, we found that all mutants were more sensitive than WT for at least one of the tested CCR peptides and the other available AMPs (**Fig. 3C,D**). The *tolB* and *tolQ* mutants were the least sensitive and displayed only a slight difference compared to WT for all tested peptides. The *dedA* and *tpr* mutants were strongly affected by the CCR1659 peptide (**Fig. 3D**) and moderately by the other tested peptides. The mutants *wzm*, *wbiF*, *wbiG*, *wbiI* and *rfbA* were sensitive to several of the tested CCRs although in many cases, enhanced sensitivity was not resulting in a complete growth inhibition but in a retarded and lesser growth compared to untreated control and the WT grown with the same peptide concentration. The *waaC* and *waaF* mutants were the most strongly affected, being more sensitive than WT to all tested peptides and at higher peptide concentrations, their growth was completely blocked (**Fig. 3D**). Taken together, the *C. insecticola* genes that were revealed by the PMB Tn-seq screen, contribute also to resistance towards other membrane-attacking AMPs, including the CCRs.

Because the tested AMPs interfere with bacterial membrane function, we characterized the cell envelope of the mutants. Since some of the mutated genes are known or suspected to be involved in LPS biosynthesis, we analyzed the LPS structure of all mutants by PAGE profiling and by mass spectrometry analysis of their lipid A moiety, which is proposed to be a direct target of PMB (*25,26*) (**Fig. 4A,B**). The *tpr*, *dedA* and *tolQ* mutants had a PAGE LPS profile that was indistinguishable from the WT. The *wzm*, *rfbA*, *wbiF*, *wbiG* and *wbiI* mutants produced a similar LPS that lacked the O-antigen but had a lipid A/core oligosaccharide moiety that was indistinguishable from WT while the *waaC* and *waaF* mutants had an altered lipid A/core moiety, in agreement with the predicted heptosyl-transferase activity of the encoded enzymes that perform the first steps of the core oligosaccharide synthesis. Mass spectrometry analysis of the lipid A moieties suggested that none of the mutants had an altered lipid A structure and notably, that all mutants produced lipid A carrying the 4-amino-4-deoxy-L arabinose (Ara4N) modification that is known to confer PMB resistance in related species (**Fig. 4B**; **fig. S7**) (*32,33,37*).

We assessed the steady-state outer membrane integrity of the mutants by NPN labeling and sensitivity to detergents (**fig. S8**). The *waaC* and *waaF* mutants had a higher NPN-derived fluorescence and slightly higher sensitivity to the non-ionic detergent Triton X100 and the

cationic detergent CTAB than the WT, while the other mutants were similar to WT. The *tolB* and *tolQ* mutants on the other hand were more sensitive to the anionic detergent SDS than to other tested strains. Overall, this indicates that although the outer membrane in some mutants has a reduced robustness, the AMP sensitivity of the mutants is not a direct consequence of a generic membrane instability but of the deficiency of specific resistance mechanisms. The capacity of the bacterial envelope to bind membrane-disrupting AMPs is a parameter influencing AMP sensitivity. The *waaC* and *wbiF* LPS mutants showed indeed a strong labeling of their envelope with CCR1659-FITC, contrary to the WT that did not show any labelling (**Fig. 4C**). However, the *tpr* mutant was also not labeled. Therefore, we quantified the relative capacity of the envelope of all the mutants to bind membrane-disrupting AMPs by labeling the cells with the fluorescent polylysine-FITC peptide or CCR1659-FITC, followed by flow cytometry analysis (**Fig. 4D**). All the mutants with altered LPS (*waaC*, *waaF*, *wzm*, *rfbA*, *wbiF*, *wbiG* and *wbiI*) had a strongly enhanced labeling with both peptides indicating a more accessible cell surface for AMP binding. However, the *dedA* and *tpr* mutants displayed a peptide labeling that was identical to the WT while the *tolB* and *tolQ* mutants were even labelled less intensively. Thus, the LPS mutants might be more sensitive to the AMPs because of the higher accessibility of their membranes for interactions with AMPs but the sensitivity of the *dedA*, *tpr* and *tolBQ* mutants has to be explained by a different mechanism. Interestingly, crypt-colonizing *C. insecticola* bacteria have lost their O-antigen after establishing in the crypts (*21*) and thus have an LPS that is similar to the LPS of the *wzm*, *rfbA*, *wbiF*, *wbiG* and *wbiI* mutants. In agreement, bacteria isolated from the crypts are hypersensitive to PMB and the CCR1659 peptide (**Fig. 3C,D**) and they strongly bind polylysine-FITC and CCR1659-FITC (**Fig. 4D**).

To confirm that the set of mutants are affected in different pathways for AMP resistance, we created the *waaC*/*tpr*, *waaC*/*dedA* and *waaC*/*wbiF* double mutants. We reasoned that if genes are part of the same pathway, double mutants should not show an additive phenotype compared to the single mutants, while in case genes are in separate pathways, double mutants might display a more severe phenotype than single mutants. We found that the three double mutants were more sensitive than the corresponding single mutants to PMB and CCR1659 and bound more CCR1659-FITC (**fig. S9**), suggesting that indeed "*waaC* and *tpr*" or "*waaC* and *dedA*" or "*waaC* and *wbiF*" define different pathways to PMB resistance. The synthetic phenotype of the *waaC*/*wbiF* mutant further suggest that the LPS core and the O-antigen constitute two distinct barriers for AMPs to reach the membrane.

SEM of untreated WT and *tpr*, *dedA*, *tolB*, *waaC* and *wzm* mutants showed that the mutants affect the bacterial envelope in various ways (**fig. S10**). SEM of CCR1659-treated cells reveals that the response to the peptide in the *waaC* and *tpr* mutant is markedly different. In the *waaC* mutant, very strong membrane distortions are visible and frequent cell lysis, indicated by the cellular material released from cells. The *tpr* mutant on the other hand shows only minor modifications on the cell surface, similar to WT, although infrequent release of large amounts of cellular material was also observed (**Fig. 4E**). Collectively, the properties of the single and double mutants suggest that in *C. insecticola* different mechanisms contribute to AMP resistance.

AMP resistance in *Caballeronia insecticola* is crucial for midgut colonization

Since the midgut crypts are the site of intensive AMP production, we next analyzed the capacity of the AMP sensitivity mutants to colonize the M4 midgut region of the *R. pedestris* midgut. As a preliminary test and to exclude that gut colonization phenotypes can be attributed to trivial reasons, we confirmed that each mutant has similar growth patterns as WT (**fig. S11A**) and is motile (**fig. S11B**) since motility is crucial for colonization of the M4 crypts (14). Analysis at 5 days post infection (dpi) of second instar nymphs showed that the 11 mutants had the capacity to colonize the crypts although they were to various extends less efficient than the WT. The WT had a 100% efficiency (n=10) and the number of bacteria per gut was consistently high ($>10^7$ genome copies per gut). In contrast, the mutants displayed a large variability in colonization level between insect individuals, ranging from a wild-type colonization level for some individuals to a failure to establish in the crypts in other individuals (**Fig. 5A**). The *waaC* and *tpr* mutants were particularly affected in agreement with their strong AMP sensitivity. This intriguing probabilistic colonization of the gut by the mutants is reminiscent to stochastic colonization of the *Drosophila* gut by underperforming *Lactobacillus plantarum* strains while a strong colonizer strain had a 100% efficiency (*38*).

Next, the fitness of the mutants in M4 colonization was evaluated when they were in competition with WT. Insects were infected with fifty-fifty mixtures of RFP-marked WT and one of the mutants (or WT as a control) that were marked with GFP. The outcome of the competitions was analyzed at 5 dpi by fluorescence microscopy of dissected M4 midguts and flow cytometry quantification of their bacterial content (**Fig. 5B**). In the control competition, RFP- and GFP-marked WT were kept in balance. However, in competitions with the mutants, the WT nearly completely outcompeted each of them, confirming their reduced colonization capacity.

Finally, we also tested if the mutants have a reduced capacity to outcompete a less efficient crypt colonizing species. We previously showed that *P. fungorum* can colonize the M4 crypts but that it is outcompeted by *C. insecticola* (13). Here, the outcompetition of *P. fungorum* by *C. insecticola* WT in co-infection experiments was confirmed while *wzm*, *waaC*, *tolB*, *tpr* and *dedA* mutants were significantly less efficient in outcompeting *P. fungorum* (**Fig. 5C**). Thus, high AMP resistance in *C. insecticola* is an important factor contributing to the efficiency of this strain in occupying the *R. pedestris* gut.

We conclude from these infection experiments that the reduced resilience to AMPs of mutants in different resistance mechanisms makes them less apt to colonize the midgut crypts. Presumably, AMP resistance is critical during the initial infection stages, from the entering of a few hundred cells into the crypt region to the rapid multiplication in two to three days of this founder population to a crypt-space-filling population of about 10^7-10^8 bacteria (*15*). Thus the surprisingly large diversity of CCR peptides, several of them already expressed in the M3 and M4 before the microbiota establishment, could be an adaptation to create a selective environment, restricting the bacteria that have a chance to establish in the M4 crypts. This mechanism could favor optimal beneficial *Caballeronia* strains among the variability of bacteria that the insect can ingest from the environment. Indeed, recent insights have changed the previous view on AMPs as generic, non-specific antimicrobials by the demonstration that they can display a degree of specificity and synergism. Accordingly, AMP repertoires in organisms dynamically evolve according to the diversity of microbes encountered in the natural environment (*39-41*). On the other hand, once established in the crypts, the bacteria lose their O-antigen by an unknown mechanism (*21*), which renders them sensitive to the CCR peptides. This suggests a second function of the CCR peptide arsenal that could be related to the protection of the crypt epithelia and prevention of the bacteria breaching these epithelia. Indeed, in *R. pedestris* the crypt epithelium lack mucus or peritrophic protective layers and is therefore in direct contact with the microbiota (*16*). Additionally, the membrane fragilization of the crypt-bacteria by the CCR peptides could facilitate the retrieval of nutrients from the bacteria (*14*), suggesting that the insect tames the gut symbionts with the CCRs.

References

1. N. A. Moran, H. Ochman, T. J. Hammer, Evolutionary and ecological consequences of gut microbial communities. *Annual Review of Ecology, Evolution, and Systematics* **50**, 451-475 (2019). doi: 10.1146/annurev-ecolsys-110617-062453.
2. J. C. Clemente, L. K. Ursell, L. W. Parfrey, R. Knight, The impact of the gut microbiota on human health: an integrative view. *Cell* **148**, 1258-1270 (2012). doi: 10.1016/j.cell.2012.01.035.
3. H. Chu, S. K. Mazmanian, Innate immune recognition of the microbiota promotes host-microbial symbiosis. *Nature Immunology* **14**, 668-675 (2013). doi: 10.1038/ni.2635.
4. L. V. Hooper, D. R. Littman, A. J. Macpherson, Interactions between the microbiota and the immune system. *Science* **336**, 1268-1273 (2012). doi: 10.1126/science.1223490.
5. J. J. Faith, J. L. Guruge, M. Charbonneau, S. Subramanian, H. Seedorf, A. L. Goodman, J. C. Clemente, R. Knight, A. C. Heath, R. L. Leibel, M. Rosenbaum, J. I. Gordon, The long-term stability of the human gut microbiota. *Science* **341**, 1237439 (2013). doi: 10.1126/science.1237439.
6. E. C. Martens, M. Neumann, M. S. Desai, Interactions of commensal and pathogenic microorganisms with the intestinal mucosal barrier. *Nature Reviews Microbiology* **16**, 457-470 (2018). doi: 10.1038/s41579-018-0036-x.
7. Z. Hu, C. Zhang, L. Sifuentes-Dominguez, C. M. Zarek, D. C. Propheter, Z. Kuang, Y. Wang, M. Pendse, K. A. Ruhn, B. Hassell, C. L. Behrendt, B. Zhang, P. Raj, T. A. Harris-Tryon, T. A. Reese, L. V. Hooper, Small proline-rich protein 2A is a gut bactericidal protein deployed during helminth infection. *Science* **374**, eabe6723 (2021). doi: 10.1126/science.abe6723.
8. D. Sun, R. Bai, W. Zhou, Z. Yao, Y. Liu, S. Tang, X. Ge, L. Luo, C. Luo, G. F. Hu, J. Sheng, Z. Xu, Angiogenin maintains gut microbe homeostasis by balancing α-Proteobacteria and Lachnospiraceae. *Gut* **70**, 666-676 (2021). doi: 10.1136/gutjnl-2019-320135.
9. R. L. Gallo, L. V. Hooper, Epithelial antimicrobial defence of the skin and intestine. *Nature Reviews Immunology* **12**, 503-516 (2012). doi: 10.1038/nri3228.
10. P. Mergaert, Role of antimicrobial peptides in controlling symbiotic bacterial populations. *Natural Product Reports* **35**, 336-356 (2018). doi: 10.1039/c7np00056a.
11. T. W. Cullen, W. B. Schofield, N. A. Barry, E. E. Putnam, E. A. Rundell, M. S. Trent, P. H. Degnan, C. J. Booth, H. Yu, A. L. Goodman, Antimicrobial peptide resistance mediates resilience of prominent gut commensals during inflammation. *Science* **347**, 170-175 (2015). doi: 10.1126/science.1260580.
12. Y. Kikuchi, T. Hosokawa, T. Fukatsu, Insect-microbe mutualism without vertical transmission: a stinkbug acquires a beneficial gut symbiont from the environment every generation. *Applied and Environmental Microbiology* **73**, 4308-4316 (2007). doi: 10.1128/AEM.00067-07. Epub 2007 May 4.
13. H. Itoh, S. Jang, K. Takeshita, T. Ohbayashi, N. Ohnishi, X. Y. Meng, Y. Mitani, Y. Kikuchi, Host-symbiont specificity determined by microbe-microbe competition in an insect gut. *Proceedings of the National Academy of Sciences USA* **116**, 22673-22682 (2019). doi: 10.1073/pnas.1912397116.
14. T. Ohbayashi, K. Takeshita, W. Kitagawa, N. Nikoh, R. Koga, X. Y. Meng, K. Tago, T. Hori, M. Hayatsu, K. Asano, Y. Kamagata, B. L. Lee, T. Fukatsu, Y. Kikuchi, Insect's intestinal organ for symbiont sorting. *Proceedings of the National Academy of Sciences USA* **112**, E5179-5188 (2015). doi: 10.1073/pnas.1511454112.
15. Y. Kikuchi, T. Ohbayashi, S. Jang, P. Mergaert, *Burkholderia insecticola* triggers midgut closure in the bean bug *Riptortus pedestris* to prevent secondary bacterial infections of

midgut crypts. *The ISME Journal* **14**, 1627-1638 (2020). doi: 10.1038/s41396-020-0633-3.
16. S. Jang, Y. Matsuura, K. Ishigami, P. Mergaert, Y. Kikuchi, Symbiont coordinates stem cell proliferation, apoptosis, and morphogenesis of gut symbiotic organ in the stinkbug-*Caballeronia* symbiosis. *Frontiers in Physiology* **13**, 1071987 (2023). doi: 10.3389/fphys.2022.1071987.
17. K. Takeshita, H. Tamaki, T. Ohbayashi, X. Y. Meng, T. Sone, Y. Mitani, C. Peeters, Y. Kikuchi, P. Vandamme, *Burkholderia insecticola* sp. nov., a gut symbiotic bacterium of the bean bug *Riptortus pedestris*. *International Journal of Systematic and Evolutionary Microbiology* **68**, 2370-2374 (2018). doi: 10.1099/ijsem.0.002848.
18. R. Futahashi, K. Tanaka, M. Tanahashi, N. Nikoh, Y. Kikuchi, B. L. Lee, T. Fukatsu, Gene expression in gut symbiotic organ of stinkbug affected by extracellular bacterial symbiont. *PLoS One* **8**, e64557 (2013). doi: 10.1371/journal.pone.0064557.
19. T. Ohbayashi, R. Futahashi, M. Terashima, Q. Barrière, F. Lamouche, K. Takeshita, X. Y. Meng, Y. Mitani, T. Sone, S. Shigenobu, T. Fukatsu, P. Mergaert, Y. Kikuchi, Comparative cytology, physiology and transcriptomics of *Burkholderia insecticola* in symbiosis with the bean bug Riptortus pedestris and in culture. *The ISME Journal* **13**, 1469-1483 (2019). doi: 10.1038/s41396-019-0361-8.
20. H. C. Clevers, C. L. Bevins, Paneth cells: maestros of the small intestinal crypts. *Annual Review of Physiology* **75**, 289-311 (2013). doi: 10.1146/annurev-physiol-030212-183744.
21. J. K. Kim, D. W. Son, C. H. Kim, J. H. Cho, R. Marchetti, A. Silipo, L. Sturiale, H. Y. Park, Y. R. Huh, H. Nakayama, T. Fukatsu, A. Molinaro, B.L. Lee, Insect gut symbiont susceptibility to host antimicrobial peptides caused by alteration of the bacterial cell envelope. *Journal of Biological Chemistry* **290**, 21042-21053 (2015). doi: 10.1074/jbc.M115.651158.
22. M. F. Burton, P. G. Steel, The chemistry and biology of LL-37. *Natural Product Reports* **26**, 1572-1584 (2009). doi: 10.1039/b912533g.
23. A. Farkas, G. Maróti, A. Kereszt, É. Kondorosi, Comparative Analysis of the Bacterial Membrane Disruption Effect of Two Natural Plant Antimicrobial Peptides. *Frontiers in Microbiology* **8**, 51 (2017). doi: 10.3389/fmicb.2017.00051.
24. S. J. Ko, E. Park, A. Asandei, J. Y. Choi, S. C. Lee, C. H. Seo, T. Luchian, Y. Park, Bee venom-derived antimicrobial peptide melectin has broad-spectrum potency, cell selectivity, and salt-resistant properties. *Scientific Reports* **10**, 10145 (2020). doi: 10.1038/s41598-020-66995-7.
25. L. Poirel, A. Jayol, P. Nordmann, Polymyxins: Antibacterial activity, susceptibility testing, and resistance mechanisms encoded by plasmids or chromosomes. *Clinical Microbiology Reviews* **30**, 557-596 (2017). doi: 10.1128/CMR.00064-16.
26. C. Ayoub Moubareck, Polymyxins and bacterial membranes: A review of antibacterial activity and mechanisms of resistance. *Membranes* **10**, 181 (2020). doi: 10.3390/membranes10080181.
27. B. P. Lazzaro, M. Zasloff, J. Rolff, Antimicrobial peptides: Application informed by evolution. *Science* **368**, eaau5480 (2020). doi: 10.1126/science.aau5480.
28. R. Spohn, L. Daruka, V. Lázár, A. Martins, F. Vidovics, G. Grézal, O. Méhi, B. Kintses, M. Számel, P. K. Jangir, B. Csörgő, Á. Györkei, Z. Bódi, A. Faragó, L. Bodai, I. Földesi, D. Kata, G. Maróti, B. Pap, R. Wirth, B. Papp, C. Pál, Integrated evolutionary analysis reveals antimicrobial peptides with limited resistance. *Nature Communications* **10**, 4538 (2019). doi: 10.1038/s41467-019-12364-6.
29. F. F. Rossetti, I. Reviakine, G. Csúcs, F. Assi, J. Vörös, M. Textor, Interaction of poly(L-lysine)-g-poly(ethylene glycol) with supported phospholipid bilayers. *Biophysical Journal* **87**, 1711-1721 (2004). doi: 10.1529/biophysj.104.041780.

30. R. Jouan, G. Lextrait, J. Lachat, A. Yokota, R. Cossard, D. Naquin, T. Timtchenko, Y. Kikuchi, T. Ohbayashi, P. Mergaert, Transposon sequencing reveals the essential gene set and genes enabling gut symbiosis in the insect symbiont *Caballeronia insecticola*. *bioRxiv* 2023.09.07.556630 (2023). doi: 10.1101/2023.09.07.556630.
31. J. K. Kim, H. A. Jang, M. S. Kim, J. H. Cho, J. Lee, F. Di Lorenzo, L. Sturiale, A. Silipo, A. Molinaro, B. L. Lee, The lipopolysaccharide core oligosaccharide of *Burkholderia* plays a critical role in maintaining a proper gut symbiosis with the bean bug *Riptortus pedestris*. *Journal of Biological Chemistry* **292**, 19226-19237 (2017). doi: 10.1074/jbc.M117.813832.
32. P. R. Panta, S. Kumar, C. F. Stafford, C. E. Billiot, M. V. Douglass, C. M. Herrera, M. S. Trent, W. T. Doerrler, A DedA family membrane protein is required for *Burkholderia thailandensis* colistin resistance. *Frontiers in Microbiology* **10**, 2532 (2019). doi: 10.3389/fmicb.2019.02532.
33. P. R. Panta, W. T. Doerrler, A link between pH homeostasis and colistin resistance in bacteria. *Scientific Reports* **11**, 13230 (2021). doi: 10.1038/s41598-021-92718-7.
34. J. K. Kim, H. Y. Park, B. L. Lee, The symbiotic role of O-antigen of *Burkholderia* symbiont in association with host *Riptortus pedestris*. *Developmental & Comparative Immunology* **60**, 202-208 (2016). doi: 10.1016/j.dci.2016.02.009.
35. B. Sit, V. Srisuknimit, E. Bueno, F. G. Zingl, K. Hullahalli, F. Cava, M. K. Waldor, Undecaprenyl phosphate translocases confer conditional microbial fitness. *Nature* **613**, 721-728 (2023). doi: 10.1038/s41586-022-05569-1.
36. J. Szczepaniak, C. Press, C. Kleanthous, The multifarious roles of Tol-Pal in Gram-negative bacteria. *FEMS Microbiology Reviews* **44**, 490-506 (2020). doi: 10.1093/femsre/fuaa018.
37. M. A. Valvano, Remodelling of the Gram-negative bacterial Kdo_2-lipid A and its functional implications. *Microbiology* **168**, 001159 (2022). doi: 10.1099/mic.0.001159.
38. B. Obadia, Z. T. Güvener, V. Zhang, J. A. Ceja-Navarro, E. L. Brodie, W. W. Ja, W. B. Ludington, Probabilistic invasion underlies natural gut microbiome stability. *Current Biology* **27**, 1999-2006 (2017). doi: 10.1016/j.cub.2017.05.034.
39. M. Zasloff, Antimicrobial peptides of multicellular organisms. *Nature* **415**, 389-395 (2002). doi: 10.1038/415389a.
40. B. P. Lazzaro, M. Zasloff, J. Rolff, Antimicrobial peptides: Application informed by evolution. *Science* **368**, eaau5480 (2020). doi: 10.1126/science.aau5480.
41. M. A. Hanson, L. Grollmus, B. Lemaitre, Ecology-relevant bacteria drive the evolution of host antimicrobial peptides in *Drosophila*. *Science* **381**, eadg5725 (2023). doi: 10.1126/science.adg5725.

Acknowledgements

We are grateful to Olga Soutourina (University Paris-Saclay, France) and Yu Matsuura (University of the Ryukyus, Japan) for critical reading of the manuscript and constructive comments. This work benefited from financial support by Saclay Plant Sciences-SPS, by the ANR grant ANR-19-CE20-0007, and by a JSPS-CNRS Bilateral Open Partnership Joint Research Project (18KK0211) and a CNRS International Research Project to Y.K. and P.M. Y.K. was supported by the MEXT KAKENHI (21K18241, 22H05068). J.L., G.L. and R.J. were supported by Ph.D. fellowships from the French Ministry of Higher Education, Research, and Innovation and A.B. benefited from a PhD contract in the frame of the CNRS 80|PRIME – 2021 program. This work was supported by JSPS Research Fellowships for Young Scientist to S.J. (21F21090), K.I. (22KJ0057) and T.O (14J03996, 20170267 and 19J01106). Tn-seq sequencing and data treatment were performed by the I2BC high-throughput sequencing facility, supported by France Génomique (funded by the French National Program Investissement d'Avenir ANR-10-INBS-09). This work has benefited from the facilities and expertise of MIMA2 (Université Paris-Saclay, INRAE, AgroParisTech, 78350, Jouy-en-Josas, France).

Author contributions

P.M. and Y.K. designed the study, planned the experiments and supervised the project. T.O., R.F, A.B. and B.A. performed transcriptome analysis. J.L., R.J., D.N. performed Tn-seq. J.L., R.J. and T.T. made mutants. P.M. and E.B. performed in vitro peptide activity assays. S.J. and K.I. provided strains. V.C. performed SEM. L.A. and P.T. performed LPS characterization. J.L., G.L., A.Y., R.C and T.O. performed insect experiments. J.L., G.L., R.J, A.B., T.O., Y.K, and P.M. analyzed data. P.M. wrote the manuscript with input from Y.K. All authors provided critical feedback and helped to shape the manuscript.

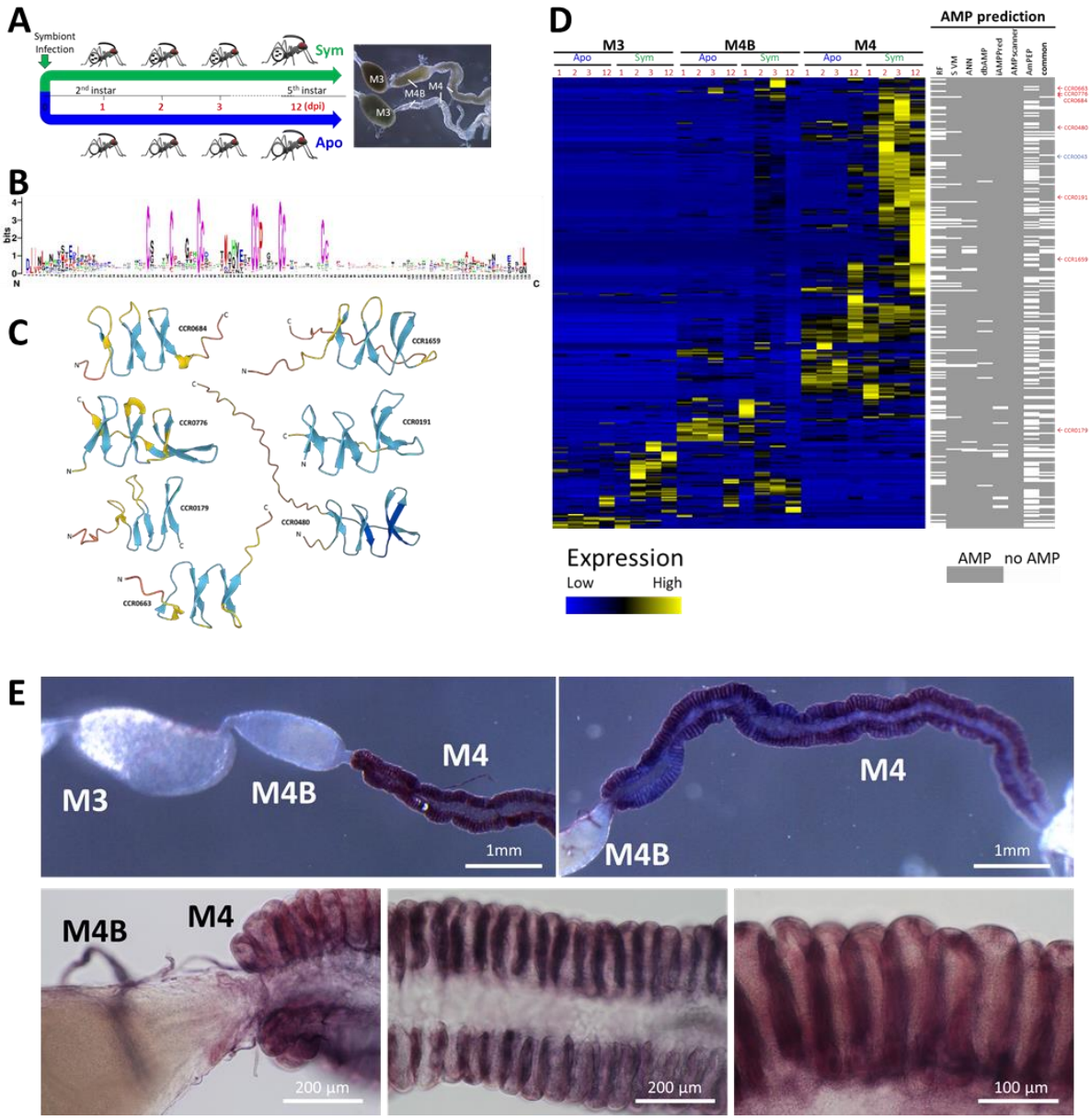

Fig. 1. CCRs are symbiosis-specific AMP-like peptides. A. Experimental setup for transcriptome analysis. First day second instars were divided in two groups. To one of them, *C. insecticola* symbionts were administered (green, Sym) and the other group remained free of symbionts (blue, Apo). Insects were dissected in the second (1, 2, and 3 days post inoculation [dpi]) or fifth instar (12 dpi) and the M3, M4B and M4 regions were harvested for transcriptome analysis. The pictures at the right show representative guts of a Sym insect at 3 dpi (top) and a same age Apo insect (bottom). **B.** Logo profile of the mature CCR peptides identified in the transcriptome, highlighting the sequence diversity of the peptides and the ten conserved cysteine residues. **C.** AlphaFold2 structural predictions of examples of CCR peptides showing antiparallel β-sheets carrying the cysteine residues. **D.** Blue-black-yellow heat map of the relative expression profile of the identified CCR genes and white-grey heat map of AMP predictions. Sample identity in the expression heat map is indicated at the top and is according to panel A. AMP prediction tools are Random Forest (RF), Support Vector Machine (SVM), Artificial Neural Network (ANN), AMPpredictor (dbAMP); iAMPpred; Antimicrobial Peptide Scanner (AMPscanner); (AmPEP_v1 and AmPEP_v2). A consensus prediction (6 out of 7 positive predictions) is indicated in the last column. The peptides used for functional

characterization are indicated at the right of the heat maps. **E.** Whole-mount *in situ* hybridization with a *CCR0043* antisense probe on the dissected midgut of a 3 dpi symbiotic insect. Positive signal appears with a blue-brownish color. CCR0043 is specifically expressed in the M4 and uniformly in all crypts. Control *in situ* hybridizations on the gut of aposymbiotic insects and with a sense probe on symbiotic insects are shown in Supplemental Figure S2.

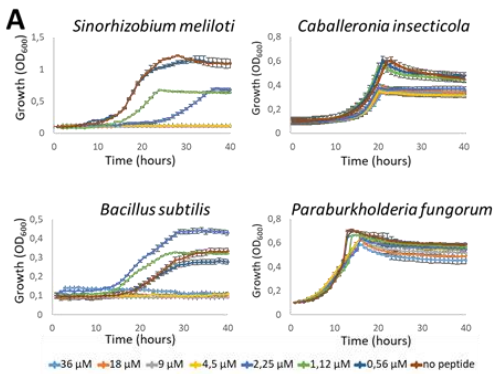

B

minimal concentration of growth inhibition (µM)	*Sinorhizobium meliloti*	*Bacillus subtilis*	*Caballeronia insecticola*	*Paraburkholderia fungorum*
PMB	1,4	2,8	22,5	90
LL37	0,69	5,56	2,78	>5,56
NCR335	1,625	>13	3,25	>13
thanatin	1,875	120	>120	>120
riptocin	<0,78	>100	50	50
CCR1659	2,25	4,5	>36	>36
CCR0191	5	10	>40	>40
CCR0179	5	20	40	40
CCR0480	<0,84375	13,5	>27	>27
CCR0663	11,25	22,5	>45	>45
CCR0684	21	10,5	>42	>42
CCR0776	40	>40	>40	>40

resistant
sensitive

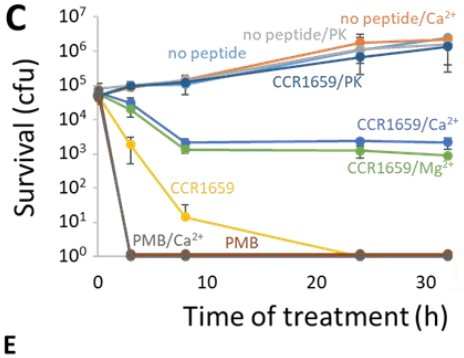

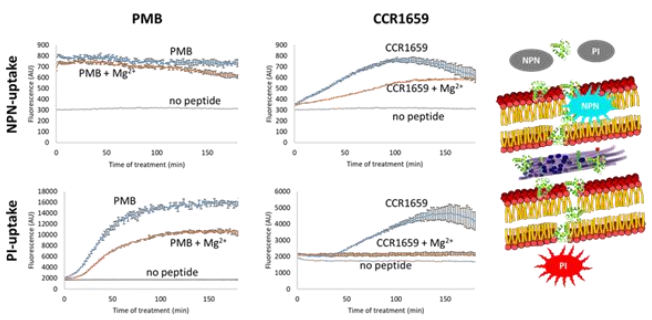

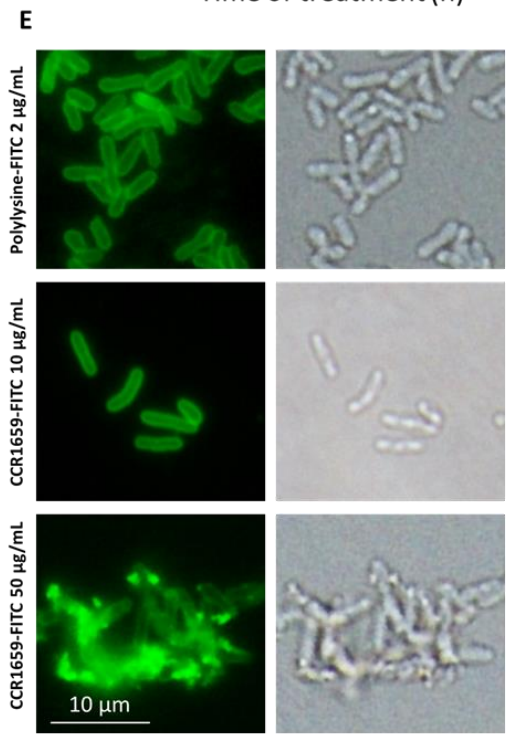

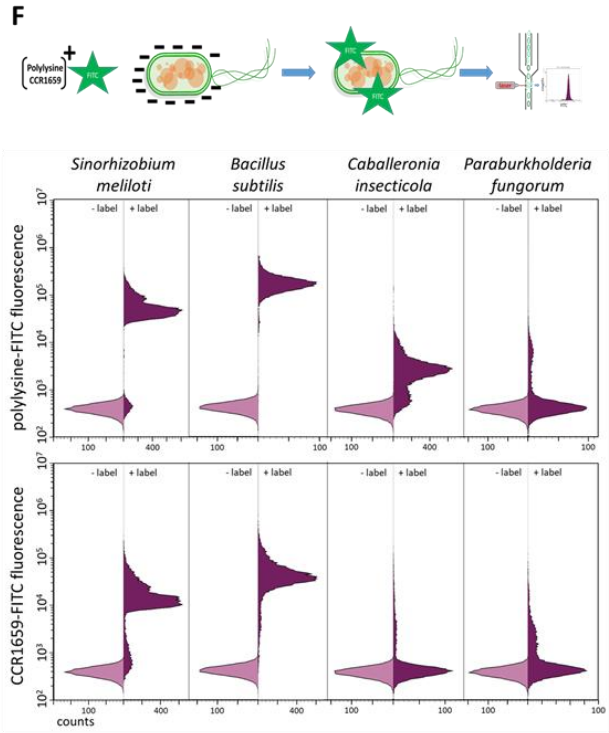

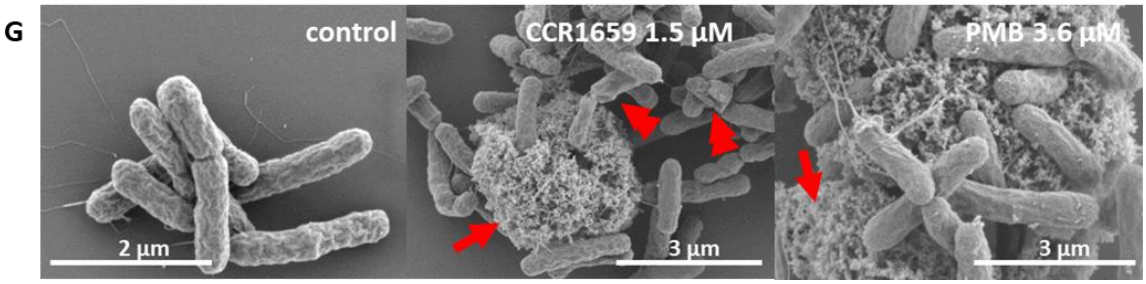

Fig. 2. CCR peptides are membrane-targeting AMPs. A. Growth inhibition of the indicated bacterial species by different concentrations of CCR1659. Error bars are standard deviations (n=3). **B.** Minimal concentrations (in µM) of growth inhibition of the indicated strains by various peptides. **C.** Bactericidal activity of 25 µM CCR1659 and 25 µM PMB. PK: proteinase K; Ca^{2+}: activity in the presence of 5 mM $CaCl_2$; Mg^{2+} activity in the presence of 5 mM $MgCl_2$. Error bars are standard deviations (n=3). **D.** NPN and PI uptake by *S. meliloti* cells in response to treatment with 10 µM CCR1659 or 10 µM PMB in the presence or absence of 5 mM $MgCl_2$. NPN is a lipophilic dye that fluoresces in hydrophobic environments such as bacterial phospholipids exposed by outer membrane damage; PI is a membrane impermeant DNA-intercalating dye that fluoresces upon DNA binding in the cytoplasm, indicative of permeabilisation of both the outer and inner membrane. Error bars are standard deviations (n=3). **E.** Fluorescence microscopy (left) of *S. meliloti* cells treated with Polylysine-FITC or CCR1659-FITC at the indicated concentrations. Corresponding bright field images are shown at the right. **F.** Flow cytometry analysis of Polylysine-FITC (top) or CCR1659-FITC binding by the indicated strains. Light purple histograms are control measurements without fluorescent label (-label); the dark purple histograms are in the presence of the fluorescent label (+label). **G.** SEM micrographs of untreated *S. meliloti* cells (left) or treated with 1.5 µM CCR1659 (middle) or with 3.6 µM PMB (right). The arrows indicate cellular material released from cells. The double arrowheads indicate cells with lost turgor.

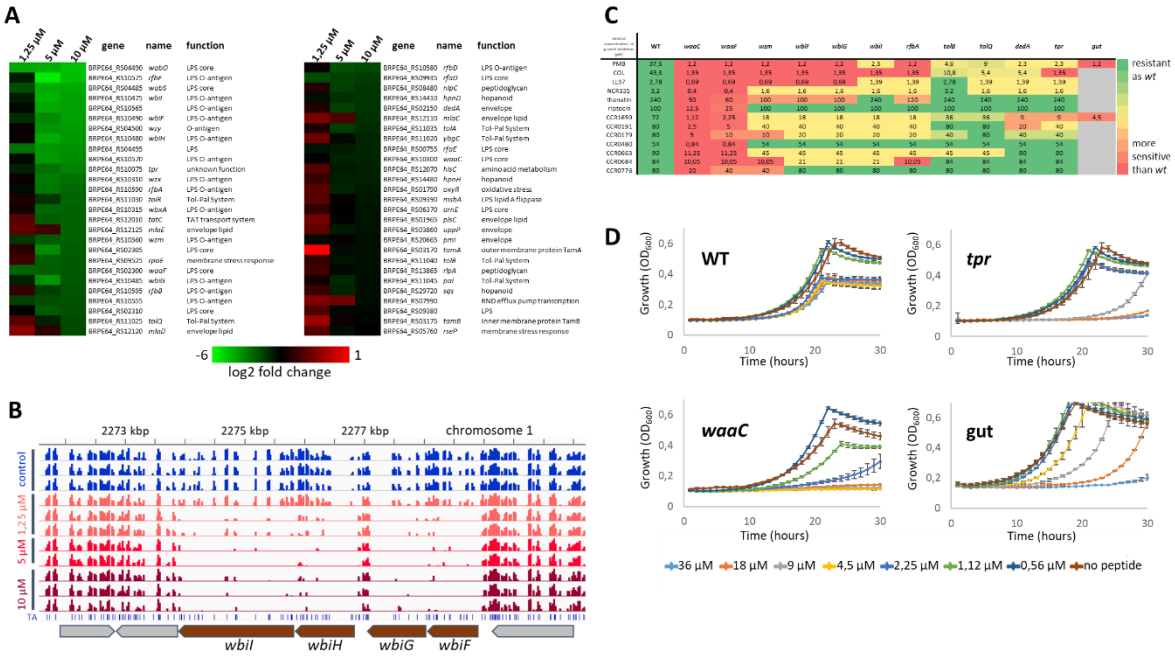

Fig. 3. Identification of AMP resistance genes by Tn-seq. A. Heat map showing the level of depletion of transposon insertions in the indicated genes in the *C. insecticola* population grown in the presence of PMB at the indicated concentrations. The color-code scale indicates the log2 fold change in the insertion abundance under the test conditions relative to the control conditions. **B.** IGV view of Tn-seq sequencing data for a selected genomic region of *C. insecticola*. The histograms indicate the abundance of mutants in the Tn-seq population for the indicated samples. Genes whose products contribute to PMB resistance have a lower frequency of Tn insertions in peptide treatment screens than in the control. **C.** Mutants in selected genes are hypersensitive to AMPs. Heat map and minimal concentrations of growth inhibition of the indicated wild-type and mutant strains by the listed peptides. Minimal concentrations are indicated in µM. The color key of the heat map is as indicated at the right. Grey cells indicate not tested. **D.** Growth inhibition of the indicated strains by different concentrations of CCR1659. Gut indicates crypt-colonizing *C. insecticola* bacteria, directly isolated from dissected M4. Error bars are standard deviations (n=3).

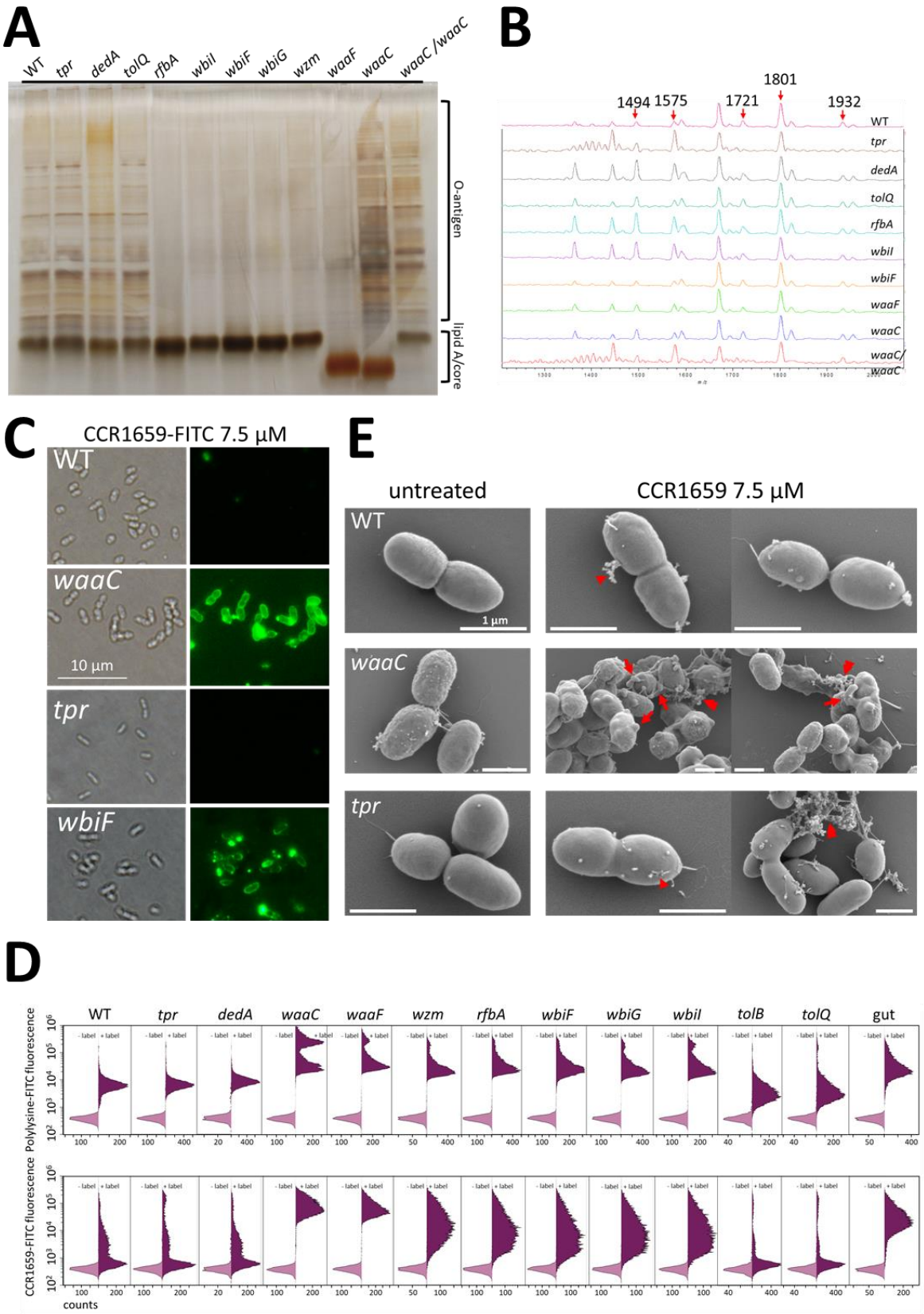

Fig. 4. Surface properties of the AMP-sensitive mutants. A. Polyacrylamide gel electrophoresis analysis of total LPS extracted from the indicated strains. The *waaC*/*waaC* strain is the complemented mutant. Despite the altered core in the *waaC* mutant, an O-antigen ladder is visible, that has a similar profile to the wild type, possibly corresponding to the O-

antigen anchored on an intermediate lipid carrier. **B.** MS analysis of the lipid A molecule present in the indicated mutants. Red arrows indicate the Ara4N carrying lipid A (Fig. S7). **C.** Fluorescence microscopy of *C. insecticola* wild-type, *waaC*, *tpr* and *wbiF* cells treated with 50 µg/mL CCR1659-FITC. All images are at the same magnification and the scalebar is 10 µm. **D.** Flow cytometry analysis of 50 µg/mL Polylysine-FITC (top) or 7.5 µM CCR1659-FITC binding by the indicated strains. Gut is bacteria directly isolated from the midgut crypts. Light purple histograms are control measurements without fluorescent label (-label); the dark purple histograms are in the presence of the fluorescent label. Note the presence of a double peak in the Polylysine-FITC treated mutants *waaC*, *waaF*, *wzm*, *rfbA*, *wbiFGI*, indicating of a heterogeneous bacterial population. **E.** SEM micrographs of untreated *C. insecticola* wild type and *waaC* and *tpr* mutant untreated cells or treated with 7.5 µM CCR1659. Arrowheads indicate release of tiny amounts of cellular material in intact cells. Double arrowheads indicate cellular material released from lysed cells. Arrows indicate cell deformations. Scale bars are 1 µm for all images.

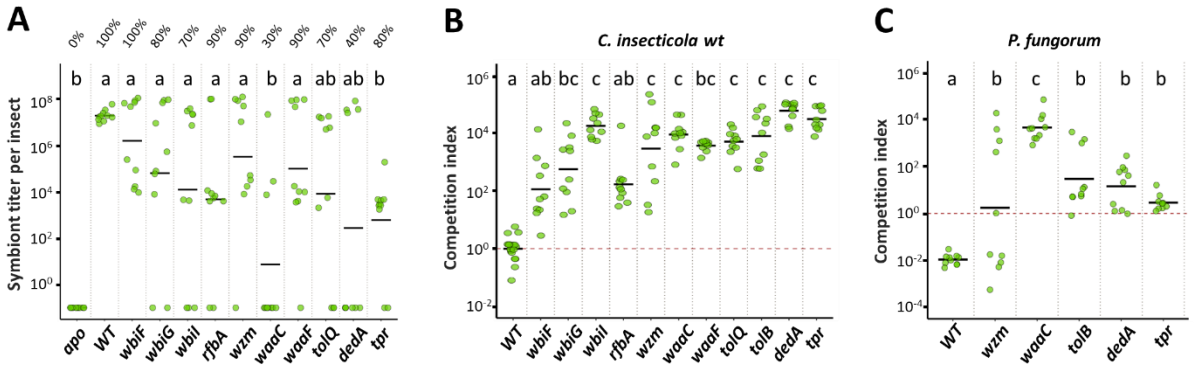

Fig. 5. AMP-sensitive mutants are impaired in gut colonization. A. Single-strain infections of *R. pedestris* second instar nymphs with *C. insecticola* WT or indicated mutants or no bacteria (*apo*). Colonization of the M4 crypt region was determined at 5 dpi by dissection and microscopy observation of the guts and symbiont titer determination by qPCR in M4 total DNA extracts. The % above the dot plots indicate the proportion of insects that showed colonization by microscopy observation (n=10). The qPCR measurements for each individual insect are indicated by green dots and the mean per mutant is indicated by a horizontal black line. **B.** Co-infections of *R. pedestris* with an equal mix of RFP-labelled *C. insecticola* WT and indicated GFP-labelled WT or mutant strains. Relative abundance of the two strains in the M4 midgut regions at 5 dpi was determined by flow cytometry on dissected intestines. The competition index expresses for all samples the ratio of WT to the indicated mutant, corrected by the ratio of the inoculum, which was in all cases close to 1. Each dot represents the competition index in an individual and the mean per mutant is indicated by a horizontal black line (n=10). **C.** Co-infections of *R. pedestris* with a 1:1 mix of GFP-labelled *P. fungorum* and indicated mScarlett-I-labelled WT or mutant *C. insecticola*. Relative abundance of the two strains in the M4 midgut regions at 5 dpi was determined by flow cytometry on dissected intestines. The competition index expresses for all samples the ratio of *P. fungorum* to the indicated mutant, corrected by the ratio of the inoculum, which was in all cases close to 1. Each dot represents the competition index in an individual and the mean per mutant is indicated by a horizontal black line (n=10). In all panels, different letters indicate statistically significant differences ($P<0.05$). Statistical significance was analyzed by Kruskal–Wallis test, Dunn *post hoc* test and Benjamini-Hochberg correction.